



# Experimental and DFT studies of the removal of pharmaceutical metronidazole from water using polypyrrole

Nouh Aarab<sup>1</sup> · Mohamed Laabd<sup>1</sup> · Habiba Eljazouli<sup>1</sup> · Rajae Lakhmiri<sup>2</sup> · Hassan Kabli<sup>1</sup> · Abdallah Albourine<sup>1</sup>

Received: 8 July 2018 / Accepted: 20 June 2019 / Published online: 29 June 2019  
© The Author(s) 2019

## Abstract

The polypyrrole (PPy) was used as an adsorbent material for efficient removal of pharmaceutical metronidazole from aqueous solutions. The physiochemical parameters influencing the adsorption process such as adsorbent dose, temperature, pH, initial concentration and contact time were systematically investigated. The optimum adsorption efficiency is achieved at pH 6.17 after 120 min of contact time. In addition, the Langmuir isotherm and pseudo-second-order models were found to explain the metronidazole adsorption process on the PPy. The thermodynamic parameters indicate that the adsorption of metronidazole on the PPy is a spontaneous and exothermic process. The quantum calculations using density functional theory (DFT) was used to confirm the adsorption mechanism of metronidazole on the PPy. The obtained results of the interaction energy indicate that the adsorption was a physical process. The metronidazole was adsorbed by its oxygen atoms on the amine groups of PPy. Finally, the PPy polymer can be used as an efficient adsorbent for removal of pharmaceutical pollutants from wastewater.

**Keywords** Adsorption · Density functional theory · Pharmaceutical metronidazole · Polypyrrole · Wastewater

## Introduction

Pharmaceutical compounds are part of the so-called emerging contaminations because of their recent interest in environmental studies. The emerging contaminants are well known as toxic and biorefractory compounds, including pharmaceuticals, pesticides, personal care products, endocrine-disrupting chemicals, and other recalcitrant organic substances [1–3]. The pharmaceutical compounds include diverse groups, such as antibiotics, hormones and anticancer agents [4, 5]. The hospitals, households and drug industries are the major sources of pharmaceutical contaminants in aquatic systems [6].

The metronidazole is an antiparasitic agent used for the treatment of *Giardia lamblia*, *Trichomonas vaginalis* and *Helicobacter pylori* infections [7, 8]. In addition, this pharmaceutical byproduct is a carcinogenic and mutagenic compound [9]. The genotoxic activity evaluation indicates that the metronidazole can induce DNA damage in human lymphocytes as well as freshwater and marine organisms [10, 11]. Therefore, its presence in water can cause harmful effects for living organisms and human health [12]. Furthermore, the metronidazole can be accumulated in the aquatic environment because of its non-biodegradability and high solubility in water [13]. For these reasons, the removal of this pollutant from wastewater is a major environmental challenge.

In this context, several decontamination methods have been developed to remove emerging contaminants from water including adsorption [14, 15], heterogeneous catalytic ozonation [16] and flocculation [17]. Among these separation technologies, the adsorption is one of the most promising techniques for removal of the pharmaceuticals from aquatic ecosystems [18]. In this regard, the use of effective adsorbent materials is necessary. Various materials such as clays [19], agricultural waste [20] and organic polymers [21, 22] were used as adsorbents for wastewater treatment.

**Electronic supplementary material** The online version of this article (<https://doi.org/10.1007/s40090-019-0190-7>) contains supplementary material, which is available to authorized users.

✉ Abdallah Albourine  
albourine.abdallah@gmail.com

<sup>1</sup> Laboratory of Materials and Environment, Faculty of Sciences, Ibn Zohr University, Agadir, Morocco

<sup>2</sup> Laboratory of Materials and Valorization of the Resources, Faculty of Sciences and Techniques, Abdelmalek Essaâdi University, Tangier, Morocco



Recently, the organic polymers (e.g., polypyrrole, polyaniline and polythiophene) were attracted considerable attention in various research fields such as gas sensors, solar cells, corrosion protection, and wastewater decontamination. [23–25]. The PPy is one of the most promising organic polymers because of its specific properties like chemical stability, biodegradability, non-toxicity, conductivity and ease of synthesis [26, 27]. The use of PPy as a novel alternative adsorbent material for removal of contaminants from water is mainly related to its large amounts of amino groups and redox reversibility [28].

The present study aims to investigate the adsorption of pharmaceutical metronidazole on the polypyrrole (PPy). The PPy was synthesized via chemical oxidative polymerization of pyrrole monomer in aqueous solution. The textural and structural properties of synthesized PPy were characterized using scanning electron microscopy (SEM) and infrared spectroscopy (IR). To find the optimum adsorption conditions, the effects of physiochemical parameters such as pH, adsorbent dose, contact time, initial concentration of metronidazole and temperature were systematically investigated. The kinetics, isotherms and thermodynamics of the metronidazole adsorption process were also studied. In addition, it was necessary to investigate the adsorption mechanism of the metronidazole on the PPy. The density functional theory (DFT) was recently used to identify the adsorption mechanism of contaminants on the conducting polymers in aqueous and gas phases [25, 29–31]. In this way, we examined the geometrical and electronic structures of PPy before and after adsorption of metronidazole using DFT to understand the mechanism involved in the adsorption process.

## Materials and methods

### Reagents

The pyrrole monomer [98% pyrrole (Aldrich)] is distilled prior to polymerization. The ferric chloride [ $\text{FeCl}_3 \cdot 6\text{H}_2\text{O}$  (Aldrich)] with strength of 0.2 M was used as an oxidant agent. The metronidazole was purchased from Sigma-Aldrich as an analytical grade reagent and used as received without further purification. The stock solution of metronidazole is obtained by dissolving 200 mg of metronidazole in 1 L of distilled water. The solutions used in the experiments were obtained by dilutions to the desired concentrations.

### Synthesis of PPy

The oxidative polymerization of pyrrole using ferric chloride was carried out according to the reaction illustrated in Fig. 1. A typical synthesis procedure can be described briefly as follows: 775  $\mu\text{l}$  of pyrrole was mixed with 37.5 ml of distilled water. Then, 12.5 ml of aqueous solution containing 0.2 M of  $\text{FeCl}_3 \cdot 6\text{H}_2\text{O}$  was gradually added to start the polymerization reaction [32]. The mixture was stirred for 2 h at room temperature. The resulting PPy was filtered on a filter paper and washed several times with distilled water and ethanol to remove the traces of unreacted products (pyrrole monomer and oxidant). Finally, the PPy was dried in an oven at 65 °C.

### Analysis method

All adsorption experiments were conducted in glass beakers containing 50 mL of metronidazole solution with constant agitation. The pH of the solution was adjusted using the solutions of HCl or NaOH. The solubility of metronidazole was mainly related to the pH of the solution. In the present work, we use a concentration of 10 mg/l (1000 times less than the solubility of metronidazole, 10.61 mg/ml at 25 °C) to investigate the effect of pH on the adsorption process [33]. In addition, the complete solubility of the metronidazole in distilled water (over the pH range of 2–12) was confirmed by UV–visible spectrophotometry. The effects of various physiochemical parameters were systematically investigated using one-variable-at-a-time experimental approach. After each adsorption test, the adsorbent was separated by membrane Millipore filters with 0.45  $\mu\text{m}$  of porosity. Then, the analysis of filtrate samples was done using UV–visible spectrophotometry (Spectrophotometer UV 2300 model) at the maximum absorption wavelength of the metronidazole (320.8 nm). The adsorbed amount and adsorption efficiency are calculated by the following equations:

Adsorbed amount in mg/g:

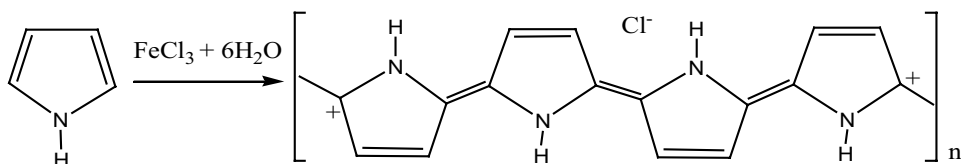
$$Q_e = ((C_0 - C_e) \times V) / m \quad (1)$$

Adsorption efficiency:

$$R(\%) = ((C_0 - C_e) / C_0) \times 100 \quad (2)$$

where  $C_0$  and  $C_e$  are the initial and equilibrium concentrations (mg/l).  $V$  and  $m$  are the volume of the solution (l) and mass of the PPy (g), respectively.

**Fig. 1** Simplified polymerization reaction of pyrrole



## Calculation methodology

The DFT calculations were performed to examine the adsorption mechanisms of metronidazole on PPy. The optimization of the molecular structures of metronidazole, PPy and their complex was performed. The energetic, structural and electronic properties of the studied molecular system at equilibrium were examined by DFT method. All quantum chemical calculations were performed using the functional hybrid B3LYP with 6–31G (d) base set implemented in *Gaussian 09* suite of program [34–37]. The GaussView 05 software was used as an interface to prepare input files and visualize the calculation results. The optimization of molecular structures is confirmed by the absence of imaginary frequencies [38–41]. To take into account the effects of the solvent (water), all calculations are carried out using the conductor-like polarizable continuum model (CPCM) as solvation model [42, 43].

The calculation of the adsorbate–adsorbent interaction energy is carried out by the following equation:

$$\Delta E_{\text{int}} = E(\text{PPy}) + E(\text{metronidazole}) - E(\text{PPy}/\text{metronidazole}) \quad (3)$$

where  $E(\text{PPy}/\text{metronidazole})$  is the energy of the complex formed between the PPy and metronidazole.  $E(\text{PPy})$  and  $E(\text{metronidazole})$  are the energies of the PPy and metronidazole, respectively.

The charge transfer ( $\Delta q$ ) between the metronidazole and PPy during the adsorption process in aqueous solution is calculated from the redistribution of the charges on the PPy before and after adsorption. The  $\Delta q$  is expressed by the Eq. (4):

$$\Delta q = q_{\text{PPy before adsorption}} - q_{\text{PPy after adsorption}} \quad (4)$$

$q_{\text{PPy before adsorption}}$  and  $q_{\text{PPy after adsorption}}$  are total net charges of the PPy before and after adsorption of metronidazole. The total net charge of the PPy was calculated from the sum of net atomic charges (Mulliken charges) of all atoms constituting the PPy.

## Results and discussion

### Characterization of the PPy

The morphology of the synthesized PPy was characterized using Field Electron and Ion Quanta 200 scanning electron microscope (SEM) instrument. Figure 2a shows the SEM micrograph of the PPy surface. From this result, it was observed that the PPy possesses a granular heterogeneous morphology. In addition, the surface of PPy exhibits

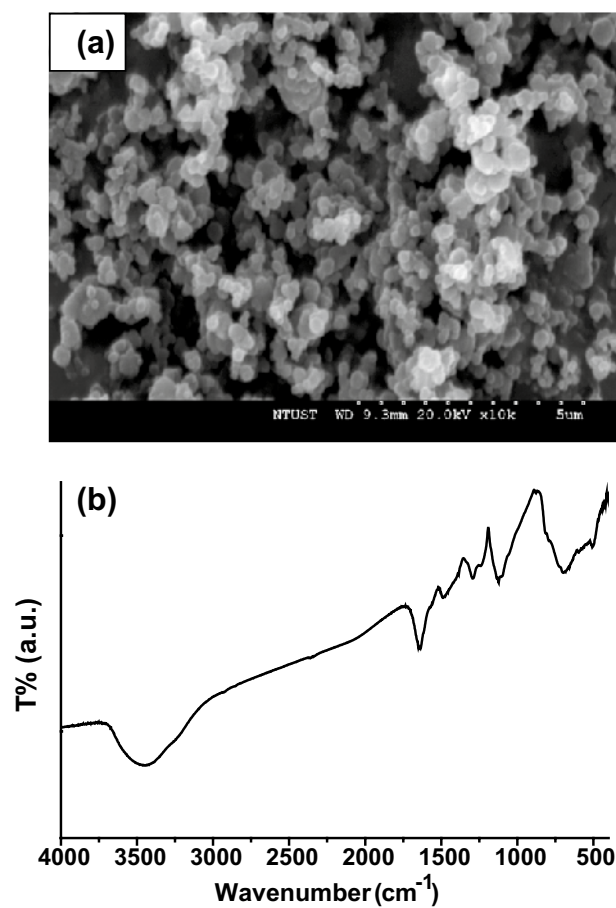


Fig. 2 a SEM micrograph, b FTIR spectrum of the synthesized PPy

a good porosity. These textural proprieties promote the diffusion of adsorbate molecules into the internal surface of PPy. Therefore, the PPy may be an efficient adsorbent material for the removal of pollutants from aqueous solutions.

The PPy was analyzed by Fourier transforms infrared spectroscopy (FTIR Vertex 70 spectrometer) over the wavenumber of 400–4000  $\text{cm}^{-1}$ . Figure 2b shows the FTIR spectrum of PPy. The broadband observed at the wavenumber of 3443  $\text{cm}^{-1}$  corresponds to the O–H stretching vibrations of the physisorbed water on the PPy surface. The peak at 1518  $\text{cm}^{-1}$  is due to the asymmetric C=C stretching vibrations of the pyrrole ring. The characteristic peak of the C–C stretching vibrations from the quinonoid structure of the pyrrole is at about 1658  $\text{cm}^{-1}$ . The peak at 1291  $\text{cm}^{-1}$  is assigned to C–N stretching vibrations of the PPy. The absorption band at 1293  $\text{cm}^{-1}$  is an indication of the in-plane C–H deformation vibrations. The peak at 824  $\text{cm}^{-1}$  can be assigned to C–H out-of-plane deformation. The C–N stretching vibration peak was observed at 1135  $\text{cm}^{-1}$ . The results revealed that the synthesized material corresponds well to the PPy [44, 45].



## Adsorption of metronidazole on the PPy

### Effect of contact time and adsorption kinetics

The effect of contact time on the removal of metronidazole by PPy was studied in the range of 0–240 min to determine the optimal required time to attain the adsorption equilibrium. Figure 3 illustrates the effect of contact time on removal efficiency of the metronidazole. From these results, it was observed that the adsorption of metronidazole was more rapid in the initial stage of the adsorption. Thereafter, the adsorption rate gradually increases with contact time until the adsorption equilibrium was established. The optimum contact time was found to be 360 min. In the beginning, the rapid metronidazole removal rate may be explained by the availability of a large number of the adsorption sites. However, the number of active sites decreases with contact time, leading to a decrease in the adsorption rate. The spectrum of metronidazole was carried out before and after adsorption (Fig. 3). As a result, we did not observe any spectral change in the positions, disappearance or appearance of new peaks. This indicates that the molecular structure of metronidazole has not changed during the adsorption process.

To determine the rate-controlling step for the adsorption of metronidazole on the PPy, the pseudo-first-order, pseudo-second-order and intraparticle diffusion models have been applied to fit the experimental data. The linear expression formulas of these kinetic models can be written in the following forms:

- Pseudo-first-order kinetic model [46]:

$$\ln(q_e - q_t) = \ln q_e - k_1 t \quad (5)$$

- Pseudo-second-order kinetic model [47]:

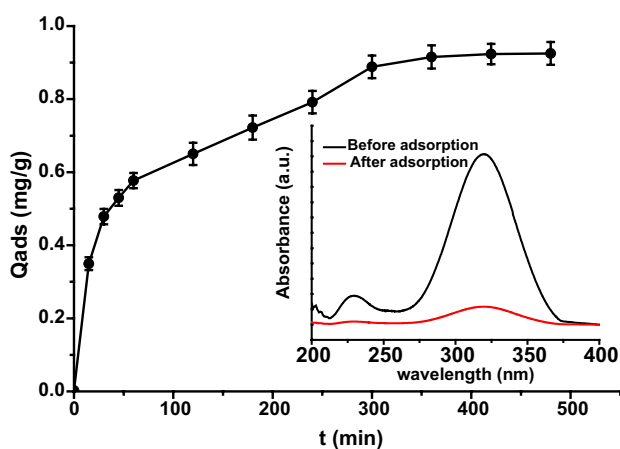


**Fig. 3** Effect of time on the adsorption of metronidazole on the PPy (adsorbent dose = 0.5 g/l,  $C_0 = 10$  mg/l, pH = 6.17 and  $T = 25$  °C)

$$t/q_t = 1/k_2 q_e^2 + t/q_e \quad (6)$$

- Intraparticle diffusion model [48]:

$$q_t = k_p t^{1/2} + C \quad (7)$$

where  $q_e$  (mg/g) and  $q_t$  (mg/g) are the adsorbed quantities at equilibrium and time  $t$ , respectively.  $k_1$  ( $\text{min}^{-1}$ ),  $k_2$  ( $\text{g}/\text{mg min}$ ) and  $k_{\text{int}}$  ( $\text{mg}/\text{g}\cdot\text{min}^{1/2}$ ) are the pseudo-first-order, pseudo-second-order and intraparticle diffusion constants, respectively.

The linear fitting of the above-presented kinetic models is shown in Fig. 4. The calculated kinetic parameters and the correlation coefficients are reported in Table 1. As seen, the values of the correlation coefficients ( $R^2$ ) indicate that the pseudo-second-order model ( $R^2 = 0.992$ ) showed a better description of the adsorption of metronidazole on the PPy compared to the pseudo-first-order model ( $R^2 = 0.867$ ). Moreover, the adsorption capacity calculated from pseudo-second-order model ( $q_{e,\text{cal}} = 1.01$  mg/g) was much closer to the experimental value ( $q_{e,\text{exp}} = 0.95$  mg/g). The diffusion mechanism of the metronidazole into PPy was investigated using the intraparticle diffusion model proposed by Weber and Morris [48]. Figure 4c illustrates the fit of the intraparticle diffusion model to the experimental data. From this figure, it was observed that the intraparticle diffusion model plot is a straight line that did not pass through the origin. This result suggests that the intraparticle diffusion is not the only process determining the adsorption of metronidazole on the PPy. Thus, the mass transfer during the adsorption process can be controlled by two mechanisms: (1) the first one represents external surface adsorption (boundary-layer diffusion); and (2) the second one represents the intraparticle diffusion and adsorption equilibrium stage [49–52].

### Effect of adsorbent dose

To examine the effect of the adsorbent dosage on the adsorption performance, the PPy dose was varied over the range of 0.05–0.70 g/l. The obtained results are illustrated in Fig. 5. As can be seen, the removal efficiency of metronidazole increases with the increase of adsorbent dose. Then, the adsorption was not significantly changed when the PPy dose reaches some value. Increase in the adsorption performance with adsorbent dose may be explained by the large adsorbent surface area and availability of more active sites of the PPy. The maximum adsorption efficiency of metronidazole obtained is 89.55% when the PPy dosage is after 0.5 g/l. In terms of maximum adsorption efficiency and cost-effectiveness, 0.5 g/l was selected as the optimum adsorbent dose for the other adsorption experiments.

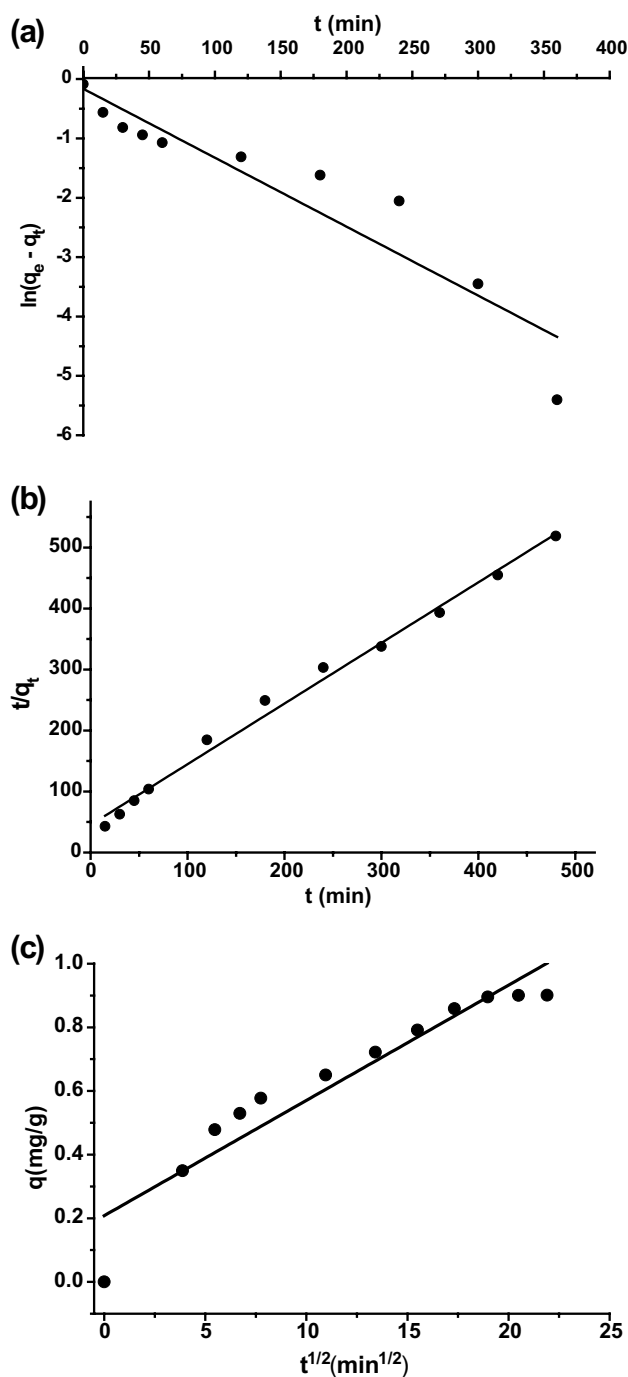


**Fig. 4** a Pseudo-first-order, b pseudo-second-order and c intraparticle diffusion plots for adsorption of metronidazole on the PPy

### Effect of pH

The pH influence on the metronidazole adsorption into PPy was studied over the pH range from 2 to 12. The pH of the solution of metronidazole was adjusted by adding NaOH or HCl. The mixtures are stirred for 360 min to ensure that the metronidazole was completely soluble [53].

**Table 1** Kinetic parameters of the adsorption of metronidazole on the PPy

Kinetic models	Parameters	
Pseudo-first order	$R^2$	0.867
	$Q_e$ (mg/g)	0.85
	$k_1$ ( $\text{min}^{-1}$ )	0.012
Pseudo-second order	$R^2$	0.992
	$Q_e$ (mg/g)	1.01
	$k_2$ (g/mg min)	0.022
Intraparticle diffusion	$R^2$	0.90
	$k_p$ (mg/g $\text{min}^{1/2}$ )	0.04
	$C$	0.21

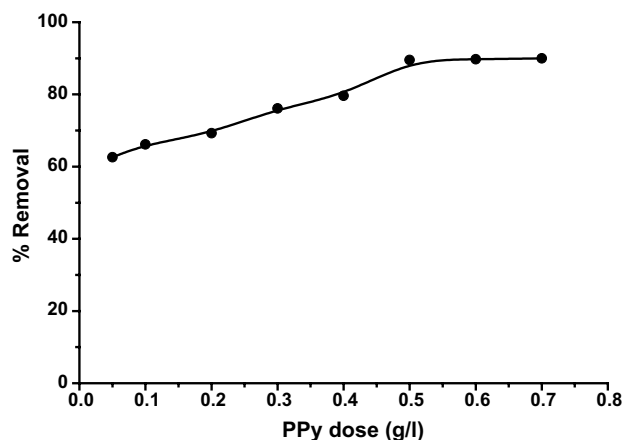


**Fig. 5** Effect of the adsorbent dose on the removal of metronidazole by PPy ( $t=360$  min,  $C_0=1$  mg/l,  $\text{pH}=6.17$  and  $T=25$  °C)

To investigate the variations in surface charge of the PPy as the pH changes, the point of zero charge ( $\text{pH}_{\text{ZPC}}$ ) was determined by immersion method as reported by Fiol and Villaescusa [54]. The  $\text{pH}_{\text{ZPC}}$  of the PPy is about 6.5. This result indicates that the PPy surface is positively charged when the pH solution is less than 6.5. Meanwhile, the PPy surface becomes negatively charged within the solution pH higher than 6.5. In addition, the metronidazole exists mainly in its deprotonated form when the pH is greater than  $\text{p}K_a$  value (2.55) [55], which comprises almost all the region studied. In contrast, the metronidazole was in its protonated form at pH less than  $\text{p}K_a$ . The effect of initial solution pH on metronidazole adsorption onto PPy is illustrated in Fig. 6. The highest adsorption efficiency of metronidazole was found when the pH is below 6. This can be rationalized by the electrostatic attractions between the positively charged PPy surface and the deprotonated metronidazole (negatively charged). However, the decrease in the adsorption efficiency with an increase in pH from 6 to 12 is probably due to the electrostatic repulsions between



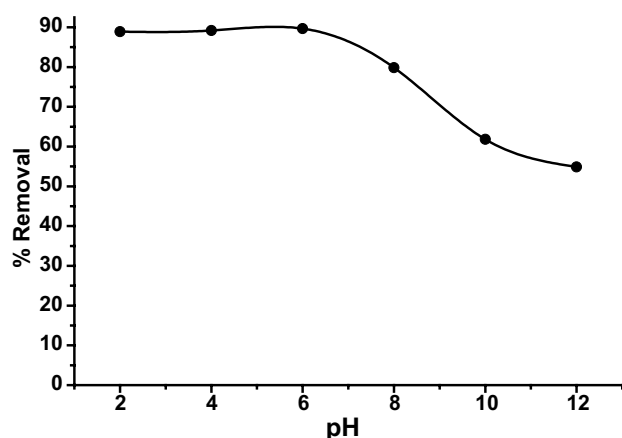


**Fig. 6** Effect of pH on the removal of metronidazole by PPy (Adsorbent dose = 0.5 g/l,  $t = 360$  min,  $C_0 = 1$  mg/l and  $T = 25$  °C)

negatively charged surface of adsorbent and deprotonated metronidazole.

### Thermodynamic parameters

The thermodynamic parameters ( $\Delta H^\circ$ ,  $\Delta S^\circ$  and  $\Delta G^\circ$ ) of the metronidazole adsorption on the PPy are related to the distribution coefficient ( $K_d$ ) of the solute between the adsorbent surface and the solution by the following equations [56]:

$$\Delta G^\circ = -RT \ln K_d \quad (8)$$

$$\ln K_d = \Delta S^\circ / R - \Delta H^\circ / RT \quad (9)$$

The coefficient of distribution  $K_d$  is defined by the equation [57]:

$$K_d = Q_e / C_e \quad (10)$$

where  $R$  (8.314 J/mol K) is the universal gas constant and  $T$  is the absolute solution temperature in Kelvin.

The values of thermodynamic parameters were determined graphically from the plot of  $\ln K_d$  versus  $1/T$ . The obtained data are shown in Table 2. The negative value of the standard enthalpy  $\Delta H^\circ$  shows that the adsorption is an exothermic process. The values of the standard free enthalpy are negative ( $\Delta G^\circ < 0$ ), demonstrating that the adsorption is a spontaneous phenomenon. In addition, the low values of  $\Delta G^\circ$  showed that the adsorption is a physisorption process [58]. The positive value of  $\Delta S^\circ$  indicates randomness at the solid–liquid interface during the adsorption process.

**Table 2** Thermodynamic parameters of the adsorption of metronidazole on the PPy

$\Delta H^\circ$ (KJ/mol)	$\Delta S^\circ$ (J/mol K)	$\Delta G^\circ$ (KJ/mol)				
		298°K	303°K	308°K	313°K	323°K
-2.854	48.85	-11.70	-11.94	-12.19	-12.43	-12.92

### Adsorption isotherms

The initial concentration is a key parameter that can significantly affect the adsorption process. The effect of the metronidazole concentration on uptake capacity was investigated in the range of 10–200 mg/l. As can be seen from Fig. 7, the metronidazole adsorption capacity increased with the initial concentration in the low concentration range. Then, the adsorbed amount grew slowly at high concentration to reach a plateau corresponding to the maximum adsorption capacity. This adsorption behavior may be due to the increase in the mass transfer driving force with increasing initial concentration [59]. Furthermore, the adsorption plateau may be explained by the fact that more active adsorption sites were being covered (saturation of the PPy) at high concentration of the metronidazole.

To obtain information on the distribution mechanism of the metronidazole on the PPy surface, the experimental equilibrium data were analyzed by Langmuir, Freundlich and Temkin isotherm models. The linear equations of the isotherm models are expressed as follows:

Langmuir model:

$$C_e / Q_e = 1 / (K_L Q_m) + C_e / Q_m \quad (11)$$

Freundlich model:

$$\ln Q_e = \ln K_f + \ln C_e / n_f \quad (12)$$

Temkin model:

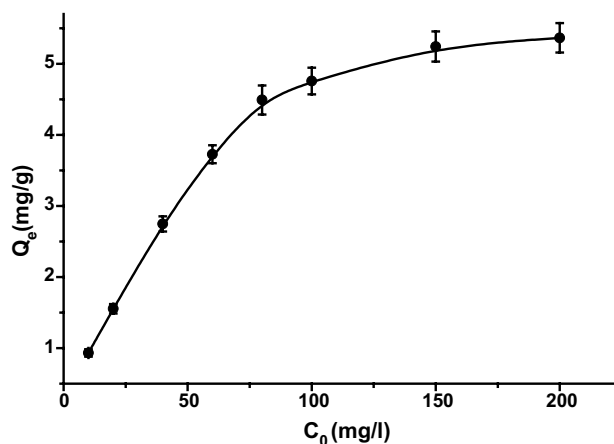


**Fig. 7** Effect of the initial concentration on the adsorbed amount of metronidazole by PPy (Adsorbent dose = 0.5 g/l,  $t = 360$  min,  $T = 25$  °C and pH = 6.17)

$$Q_e = B_T \ln K_T + B_T \ln C_e \quad (13)$$

where  $K_L$  is the Langmuir binding constant,  $C_e$  (mg/l) is the equilibrium concentration,  $Q_e$  (mg/g) is the adsorbed amount at equilibrium,  $Q_m$  (mg/g) is the maximum adsorption capacity,  $K_f$  and  $n$  are the Freundlich empirical constants,  $K_T$  and  $B$  are the Temkin Constants.

The separation factor is a dimensionless constant that allows predicting the feasibility of the adsorption process [60]. From Langmuir isotherm, the separation factor ( $R_L$ ) is calculated using the equation:

$$R_L = \frac{1}{1 + K_L C_0} \quad (14)$$

where  $C_0$  is the initial concentration of metronidazole and  $K_L$  is the Langmuir binding constant. If  $R_L > 1$ , this indicates that the adsorption is not favorable. If  $0 < R_L < 1$ , this suggests that the adsorption is favorable. If  $R_L = 1$ , it means linear adsorption.

The graphical presentations of the Langmuir, Freundlich and Temkin adsorption isotherms are represented in Fig. 8. The values of the equilibrium parameters and correlation coefficients ( $R^2$ ) generated by linear regression analysis are given in Table 3. As can be seen from Table 3, the experimental data were best fitted to the Langmuir isotherm model when the correlation coefficient values ( $R^2$ ) are compared. In addition, the maximum adsorption capacity calculated by Langmuir isotherm (5.05 mg/g) is close to that obtained experimentally (5.36 mg/g). Moreover, the value of the separation factor ( $0 < R_L < 1$ ) indicates that the adsorption of metronidazole into PPy is favorable [61]. The value of  $1/n$  ( $=0.365$ ) indicates high adsorption affinity between PPy and metronidazole. Thus, the metronidazole adsorption on the PPy is a monolayer process that occurs on the identical active sites.

## DFT study of the adsorption of metronidazole on the PPy

### Electronic density distribution

The distribution of electron density on the optimized geometries of the adsorbate and adsorbent molecules was calculated to identify the nucleophilic and electrophilic attack sites. Figure 9 illustrates the MEP (molecular electrostatic potential) of PPy and the metronidazole. The results obtained show that the oxygenated groups of metronidazole have a high negative electron density and delocalized on these functional groups (red color). This indicates that these groups may be considered as nucleophilic attack sites for the metronidazole molecules. On the other hand, the amine

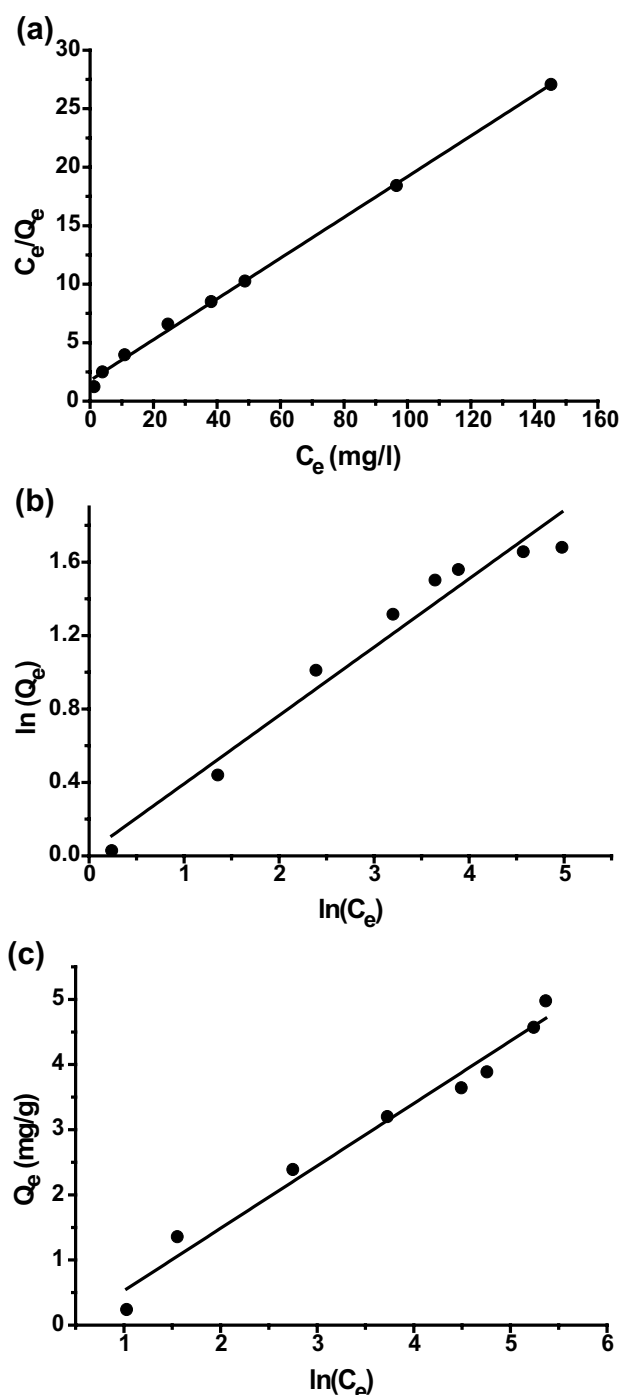


**Fig. 8** a Langmuir, b Freundlich and c Temkin isotherm plots for the adsorption of metronidazole on the PPy

functional groups of tripyrrole lead to a high positive electron density (blue color). This suggests that the amine groups are the electrophilic attack sites for the PPy. According to these results, the adsorption mechanism of metronidazole on the PPy can be carried out through interactions between



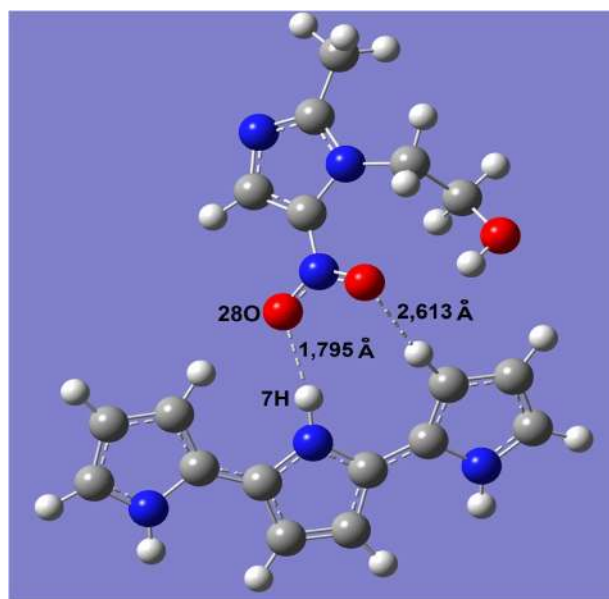
**Table 3** Langmuir, Freundlich and Temkin isotherm constants for adsorption of metronidazole on the PPy

Isotherm models	Parameters	
Langmuir	$Q_m$ (mg/g)	5.05
	$K_L$ (l/mg)	0.001
	$R^2$	0.981
	$R_L$	0.83
Freundlich	$K_f$	1.118
	$n$	2.740
	$R^2$	0.950
Temkin	$B$	0.696
	$K_T$ (l/mg)	2.022
	$R^2$	0.976

the nucleophilic (containing oxygen atoms) and electrophilic ( $-NH-$ ) groups.

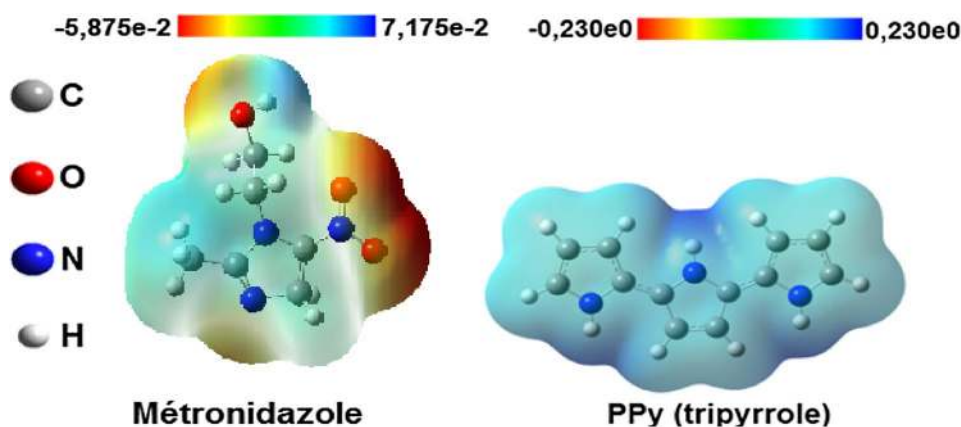
### Charge transfer

The charge transfer phenomenon between the molecules at the solute/adsorbent interface is examined by analysis of the net atomic charges of the PPy before and after complexation/adsorption with metronidazole (Table S1). The results were obtained after optimization of the complex formed between tripyrrole and metronidazole. The redistribution of net charges indicates that the metronidazole loses electrical charges of the order of 0.137e. This loss is transferred to the PPy during the adsorption process. In addition, this low electronic density suggests that the adsorption of metronidazole on the PPy is a physisorption type [62]. This is in good agreement with the experimental results obtained previously.

**Fig. 10** Optimized molecular geometry of the complex formed between tripyrrole and metronidazole

### Intermolecular distances

Figure 10 shows the optimized molecular geometry of the PPy/metronidazole complex. The distances between the two molecules were calculated. The obtained results indicate that there is a short distance (1.795 Å) between the oxygen atom (28O) of metronidazole and the hydrogen (7H) substituted on the nitrogen atom of the PPy. According to International Union of Pure and Applied Chemistry, hydrogen bonds were defined as the electrostatic donor–acceptor interactions between a hydrogen atom (attached to an electronegative atom) and an electronegative atom [63]. The lengths of hydrogen bonds are typically between 1.4 and 3.3 Å. Thus, the intermolecular interactions between the metronidazole and PPy lead to

**Fig. 9** Distribution of the electron density on the optimized molecular geometries of the PPy (tripyrrrole) and metronidazole



the formation of hydrogen bonds during the adsorption process. This suggests that the adsorption mechanism is essentially a physical process, which is in good adequacy with above-presented experimental results.

### Interaction energy

The calculation of the formation/interaction energies ( $\Delta E_{\text{int}}$ ) is very important to study the interactions between the adsorbent material and adsorbate molecule to evaluate the stability of the obtained complex [64, 65]. The value of the interaction energy during the formation of PPy/metronidazole system is equal to  $-0.163$  u.a. This result confirms that metronidazole molecules present a good affinity on the PPy. In addition, the low value of  $\Delta E_{\text{int}}$  shows that metronidazole adsorbs physically on the PPy surface. This confirms that the adsorption process is favorable.

### Conclusion

The PPy was synthesized and used as an adsorbent for removal of metronidazole from aqueous solutions. The effect of contact time on the adsorption of metronidazole on the PPy shows that the equilibrium time does not exceed 360 min. The maximum adsorption efficiency was obtained for a PPy dosage of 0.5 g/l, while the optimum agitation time and pH were 360 min and 6.17, respectively. The adsorption kinetics data were best described by the pseudo-second-order model. The equilibrium adsorption data were found to agree best with the Langmuir model. The thermodynamic parameters suggest that the adsorption is a spontaneous and exothermic process. The quantum chemical calculations using DFT method showed that the adsorption mechanism of metronidazole on the PPy was mainly governed by physical interactions at solid/liquid interface. Overall, the PPy can be used as an eco-friendly and effective adsorbent material for the removal of metronidazole and eventually other pharmaceutical pollutants from the hospital and municipal wastewaters.

### Compliance with ethical standards

**Conflict of interest** On behalf of all authors, the corresponding author states that there is no conflict of interest.

**Open Access** This article is distributed under the terms of the Creative Commons Attribution 4.0 International License (<http://creativecommons.org/licenses/by/4.0/>), which permits unrestricted use, distribution, and reproduction in any medium, provided you give appropriate credit to the original author(s) and the source, provide a link to the Creative Commons license, and indicate if changes were made.

### References

1. Wang JL, Wang SZ (2016) Removal of pharmaceuticals and personal care products (PPCPs) from wastewater: a review. *J Environ Manag* 182:620–640. <https://doi.org/10.1016/j.jenvman.2016.07.049>
2. Schwarzenbach RP, Escher BI, Fenner K, Hofstetter TB, Johnson CA, von Gunten U, Wehrli B (2006) The challenge of micropollutants in aquatic systems. *Science* 313:1072–1077. <https://doi.org/10.1126/science.1127291>
3. Wilkinson JL, Hooda PS, Barker J, Barton S, Swinden J (2016) Ecotoxic pharmaceuticals, personal care products, and other emerging contaminants: a review of environmental, receptor-mediated, developmental, and epigenetic toxicity with discussion of proposed toxicity to humans. *Crit Rev Environ Sci Technol* 46:336–381. <https://doi.org/10.1080/10643389.2015.1096876>
4. Schwarzenbach RP, Egli T, Hofstetter TB, von Gunten U, Wehrli B (2010) Global water pollution and human health. *Annu Rev Environ Resour* 35:109–136. <https://doi.org/10.1146/annurev-environ-100809-125342>
5. Luo S, Wei Z, Spinney R, Zhang Z, Dionysiou DD, Gao L, Chai L, Wang D, Xiao R (2018) UV direct photolysis of sulfamethoxazole and ibuprofen: an experimental and modelling study. *J Hazard Mater* 343:132–139. <https://doi.org/10.1016/j.jhazmat.2017.09.019>
6. Nazari G, Abolghasemi H, Esmaili M (2016) Batch adsorption of cephalixin antibiotic from aqueous solution by walnut shell-based activated carbon. *J Taiwan Inst Chem Eng* 58:357–365. <https://doi.org/10.1016/j.jtice.2015.06.006>
7. Bahmani M, Saki K, Rafieian-Kopaei M, Karamati SA, Eftekhari Z, Jelodar M (2014) The most common herbal medicines affecting *Sarcomastigophora* branches: a review study. *Asian Pac J Trop Med* 7:S14–S21. [https://doi.org/10.1016/s1995-7645\(14\)60198-x](https://doi.org/10.1016/s1995-7645(14)60198-x)
8. Mabe K, Okuda M, Kikuchi S, Amagai K, Yoshimura R, Kato M, Sakamoto N, Asaka M, Japan Gast Study Group (2018) Randomized controlled trial: PPI-based triple therapy containing metronidazole versus clarithromycin as first-line treatment for *Helicobacter pylori* in adolescents and young adults in Japan. *J Infect Chemother* 24:538–543. <https://doi.org/10.1016/j.jiac.2018.02.013>
9. Daeseleire E, Ruyck H, Van Renterghem R (2000) Rapid confirmatory assay for the simultaneous detection of ronidazole, metronidazole and dimetridazole in eggs using liquid chromatography–tandem mass spectrometry. *Analyst* 125:1533–1535. <https://doi.org/10.1039/b005707j>
10. Ré JL, De Méo MP, Laget M, Guiraud H, Castegnaro M, Vanelle P, Duménil G (1997) Evaluation of the genotoxic activity of metronidazole and dimetridazole in human lymphocytes by the comet assay. *Mutat Res* 375:147–155
11. Lanzky PF, Haning-Snrensen B (1997) The toxic effect of the antibiotic metronidazole on aquatic organisms. *Chemosphere* 35:2553–2561
12. Daeseleire E, Ruyck H, Van Renterghem R (2000) Rapid confirmatory assay for the simultaneous detection of ronidazole, metronidazole and dimetridazole in eggs using liquid chromatography–tandem mass spectrometry. *Analyst* 125:1533–1535. <https://doi.org/10.1039/b005707j>
13. Kümmerer K, Al-Ahmad A, Mersch-Sundermann V (2000) Biodegradability of some antibiotics, elimination of the genotoxicity and affection of wastewater bacteria in a simple test. *Chemosphere* 40:701–710. [https://doi.org/10.1016/s0045-6535\(99\)00439-7](https://doi.org/10.1016/s0045-6535(99)00439-7)
14. Ling Y, Klemes MJ, Xiao L, Alsbaiee A, Dichtel WR, Helbling DE (2017) Benchmarking micropollutant removal by activated carbon and porous  $\beta$ -cyclodextrin polymers under environmentally



- relevant scenarios. *Environ Sci Technol* 51:7590–7598. <https://doi.org/10.1021/acs.est.7b00906>
15. Alsbaiee A, Smith BJ, Xiao L, Ling Y, Helbling DE, Dichtel WR (2015) Rapid removal of organic micropollutants from water by a porous  $\beta$ -cyclodextrin polymer. *Nature* 529:190–194. <https://doi.org/10.1038/nature16185>
  16. Wang J, Bai Z (2017) Fe-based catalysts for heterogeneous catalytic ozonation of emerging contaminants in water and wastewater. *Chem Eng J* 312:79–98. <https://doi.org/10.1016/j.cej.2016.11.118>
  17. Mohammed N, Grishkewich N, Tam KC (2018) Cellulose nanomaterials: promising sustainable nanomaterials for application in water/wastewater treatment processes. *Environ Sci Nano* 5:623–658. <https://doi.org/10.1039/c7en01029j>
  18. Worch E (2012) Adsorption technology in water treatment: fundamentals, processes, and modeling. Walter de Gruyter, Göttingen
  19. Zhu R, Chen Q, Zhou Q, Xi Y, Zhu J, He H (2016) Adsorbents based on montmorillonite for contaminant removal from water: a review. *Appl Clay Sci* 123:239–258. <https://doi.org/10.1016/j.clay.2015.12.024>
  20. Habineza A, Zhai J, Ntakirutimana T, Qiu FP, Li X, Wang Q (2017) Heavy metal removal from wastewaters by agricultural waste low-cost adsorbents: hindrances of adsorption technology to the large scale industrial application—a review. *Desalin Water Treat* 78:192–214. <https://doi.org/10.5004/dwt.2017.20581>
  21. Xiao L, Ling Y, Alsbaiee A, Li C, Helbling DE, Dichtel WR (2017)  $\beta$ -Cyclodextrin polymer network sequesters perfluorooctanoic acid at environmentally relevant concentrations. *J Am Chem Soc* 139:7689–7692. <https://doi.org/10.1021/jacs.7b02381>
  22. Klemes MJ, Ling Y, Chiapasco M, Alsbaiee A, Helbling DE, Dichtel W (2018) Phenolation of cyclodextrin polymers controls their lead and organic micropollutant adsorption. *Chem Sci* 9:8883–8889. <https://doi.org/10.1039/c8sc03267j>
  23. Laabd M, Chafai H, Aarab N, El Jaouhari A, Bazzaoui M, Kabli H, Eljazouli H, Albourine A (2016) Polyaniline films for efficient removal of aromatic acids from water. *Environ Chem Lett* 14:395–400. <https://doi.org/10.1007/s10311-016-0569-z>
  24. Xiao R, Luo Z, Wei Z, Luo S, Spinney R, Yang W, Dionysiou DD (2018) Activation of peroxymonosulfate/persulfate by nanomaterials for sulfate radical-based advanced oxidation technologies. *Curr Opin Chem Eng* 19:51–58. <https://doi.org/10.1016/j.coche.2017.12.005>
  25. Laabd M, El Jaouhari A, Bazzaoui M, Albourine A, El Jazouli H (2017) Adsorption of benzene-polycarboxylic acids on the electro-synthesized polyaniline films: experimental and DFT calculation. *J Polym Environ* 25:359–369. <https://doi.org/10.1007/s10924-016-0814-3>
  26. Chafai H, Laabd M, Elbariji S, Bazzaoui M, Albourine A (2016) Study of congo red adsorption on the polyaniline and polypyrrole. *J Dispers Sci Technol* 38:832–836. <https://doi.org/10.1080/01932691.2016.1207185>
  27. Tabačiarová J, Mičušík M, Fedorko P, Omastová M (2015) Study of polypyrrole aging by XPS, FTIR and conductivity measurements. *Polym Degrad Stab* 120:392–401. <https://doi.org/10.1016/j.polymdegradstab.2015.07.021>
  28. Katal R, Ghiass M, Esfandian H (2011) Application of nanometer size of polypyrrole as a suitable adsorbent for removal of Cr(VI). *J Vinyl Addit Technol* 17:222–230. <https://doi.org/10.1002/vnl.20287>
  29. Mahto TK, Chandra S, Halder C, Sahu SK (2015) Kinetic and thermodynamic study of polyaniline functionalized magnetic mesoporous silica for magnetic field guided dye adsorption. *RSC Adv* 5:47909–47919. <https://doi.org/10.1039/c5ra08284f>
  30. Shokuhi Rad A, Zardoost MR, Abedini E (2015) First-principles study of terpyrrole as a potential hydrogen cyanide sensor: DFT calculations. *J Mol Model* 21:273–278. <https://doi.org/10.1007/s00894-015-2814-y>
  31. Ullah H, Shah AHA, Bilal S, Ayub K (2013) DFT study of polyaniline NH<sub>3</sub>, CO<sub>2</sub>, and CO gas sensors: comparison with recent experimental data. *J Phys Chem C* 117:23701–23711. <https://doi.org/10.1021/jp407132c>
  32. Laabd M, El Jaouhari A, Ait Haki M, Eljazouli H, Bazzaoui M, Kabli H, Albourine A (2016) Simultaneous removal of benzene polycarboxylic acids from water by polypyrrole composite filled with a cellulosic agricultural waste. *J Environ Chem Eng* 4:1869–1879. <https://doi.org/10.1016/j.jece.2016.03.015>
  33. Di Martino P, Censi R, Malaj L, Capsoni D, Massarotti V, Martelli S (2007) Influence of solvent and crystallization method on the crystal habit of metronidazole. *Cryst Res Technol* 42:800–806. <https://doi.org/10.1002/crat.200710908>
  34. Frisch MJ et al (2009) GAUSSIAN 09, Rev. D.01. Gaussian Inc, Wallingford
  35. Xiao R, Gao L, Wei Z, Spinney R, Luo S, Wang D, Dionysiou DD, Tang CJ, Yang W (2017) Mechanistic insight into degradation of endocrine disrupting chemical by hydroxyl radical: an experimental and theoretical approach. *Environ Pollut* 231:1446–1452. <https://doi.org/10.1016/j.envpol.2017.09.006>
  36. Ye T, Wei Z, Spinney R, Tang CJ, Luo S, Xiao R, Dionysiou DD (2017) Chemical structure-based predictive model for the oxidation of trace organic contaminants by sulfate radical. *Water Res* 116:106–115. <https://doi.org/10.1016/j.watres.2017.03.015>
  37. Yang Z, Su R, Luo S, Spinney R, Cai M, Xiao R, Wei Z (2017) Comparison of the reactivity of ibuprofen with sulfate and hydroxyl radicals: an experimental and theoretical study. *Sci Total Environ* 590–591:751–760. <https://doi.org/10.1016/j.scitotenv.2017.03.039>
  38. Luo S, Wei Z, Spinney R, Yang Z, Chai L, Xiao R (2017) A novel model to predict gas–phase hydroxyl radical oxidation kinetics of polychlorinated compounds. *Chemosphere* 172:333–340. <https://doi.org/10.1016/j.chemosphere.2017.01.014>
  39. Luo S, Wei Z, Spinney R, Villamena FA, Dionysiou DD, Chen D, Tang CJ, Chai L, Xiao R (2018) Quantitative structure–activity relationships for reactivities of sulfate and hydroxyl radicals with aromatic contaminants through single–electron transfer pathway. *J Hazard Mater* 344:1165–1173. <https://doi.org/10.1016/j.jhazmat.2017.09.024>
  40. Luo S, Wei Z, Dionysiou DD, Spinney R, Hu WP, Chai L, Yang Z, Ye T, Xiao R (2017) Mechanistic insight into reactivity of sulfate radical with aromatic contaminants through single–electron transfer pathway. *Chem Eng J* 327:1056–1065. <https://doi.org/10.1016/j.cej.2017.06.179>
  41. Luo S, Gao L, Wei Z, Spinney R, Dionysiou DD, Hu WP, Chai L, Xiao R (2018) Kinetic and mechanistic aspects of hydroxyl radical-mediated degradation of naproxen and reaction intermediates. *Water Res* 137:233–241. <https://doi.org/10.1016/j.watres.2018.03.002>
  42. Cossi M, Barone VJ (2001) Time-dependent density functional theory for molecules in liquid solutions. *Chem Phys* 115:4708–4717. <https://doi.org/10.1063/1.1394921>
  43. Cossi M, Rega N, Scalmani G, Barone V (2003) Energies, structures, and electronic properties of molecules in solution with the C-PCM solvation model. *J Comput Chem* 24:669–681. <https://doi.org/10.1002/jcc.10189>
  44. Feng JT, Li JJ, Lv W, Xu H, Yang HH, Yan W (2014) Synthesis of polypyrrole nano-fibers with hierarchical structure and its adsorption property of acid red G from aqueous solution. *Synth Met* 191:66–73. <https://doi.org/10.1016/j.synthmet.2014.02.013>
  45. Zhang X, Wu X, Lu C, Zhou Z (2015) Dialysis-free and in situ doping synthesis of polypyrrole@ cellulose nanowhiskers nanohybrid for preparation of conductive nanocomposites with enhanced properties. *ACS Sustainable Chem Eng* 3:675–682. <https://doi.org/10.1021/sc500853m>

46. Langergren S, Svenska B (1898) The theory of adsorption of solutes. *Veternskaps Akad Handl* 24:1–39
47. Ho YS, McKay G (1998) Kinetic models for the sorption of dye from aqueous solution by wood. *Process Saf Environ Prot* 78:183–191
48. Weber WJ, Morris JC (1963) Kinetics of adsorption on carbon from solution. *ASCE Sanit Eng Div J* 1:1–2
49. Naseeruteen F, Hamid NSA, Suah FBM, Ngah WSW, Mehamod FS (2018) Adsorption of malachite green from aqueous solution by using novel chitosan ionic liquid beads. *Int J Biol Macromol* 107:1270–1277. <https://doi.org/10.1016/j.ijbiomac.2017.09.111>
50. Pholosi A, Naidoo BE, Ofomaja AE (2019) Enhanced arsenic (iii) adsorption from aqueous solution by magnetic pine cone biomass. *Mater Chem Phys* 222:20–30. <https://doi.org/10.1016/j.matchemphys.2018.09.067>
51. Khamirchi R, Hosseini-Bandegharai A, Alahabadi A, Sivamani S, Rahmani-Sani A, Shahryari T, Anastopoulos I, Miri M, Tran HN (2018) Adsorption property of Br-PADAP-impregnated multiwall carbon nanotubes towards uranium and its performance in the selective separation and determination of uranium in different environmental samples. *Ecotoxicol Environ Saf* 150:136–143. <https://doi.org/10.1016/j.ecoenv.2017.12.039>
52. Apul OG, Shao T, Zhang SJ, Karanfil T (2012) Impact of carbon nanotube morphology on phenanthrene adsorption. *Environ Toxicol Chem* 31:73–78. <https://doi.org/10.1002/etc.705>
53. Cho MJ, Kurtz RR, Lewis C, Machkovech SM, Houser DJ (1982) Metronidazole phosphate—a water-soluble prodrug for parenteral solutions of metronidazole. *J Pharm Sci* 71:410–414. <https://doi.org/10.1002/jps.2600710409>
54. Fiol N, Villaescusa I (2009) Determination of sorbent point zero charge: usefulness in sorption studies. *Environ Chem Lett* 7:79–84. <https://doi.org/10.1007/s10311-008-0139-0>
55. Shemer H, Kunukcu YK, Linden KG (2006) Degradation of the pharmaceutical metronidazole via UV, Fenton and photo-Fenton processes. *Chemosphere* 63:269–276. <https://doi.org/10.1016/j.chemosphere.2005.07.029>
56. Nandi BK, Goswami A, Purkait MK (2009) Removal of cationic dyes from aqueous solutions by kaolin: kinetic and equilibrium studies. *Appl Clay Sci* 42:583–590. <https://doi.org/10.1016/j.clay.2008.03.015>
57. Eren E, Afsin B, Onal Y (2009) Removal of lead ions by acid activated and manganese oxide-coated bentonite. *J Hazard Mater* 161:677–685. <https://doi.org/10.1016/j.jhazmat.2008.04.020>
58. Seki Y, Yurdakoc K (2006) Adsorption of promethazine hydrochloride with KSF montmorillonite. *Adsorption* 12:89–100. <https://doi.org/10.1007/s10450-006-0141-4>
59. Tighadouini S, Radi S, Bacquet M, Degoutin S, Zaghrioui M, Jodeh S, Warad I (2016) Removal efficiency of Pb(II), Zn(II), Cd(II) and Cu(II) from aqueous solution and natural water by ketoenol-pyrazole receptor functionalized silica hybrid adsorbent. *Sep Sci Technol* 52:608–621. <https://doi.org/10.1080/01496395.2016.1262874>
60. Jodeh S, Hamed O, Melhem A, Salghi R, Jodeh D, Azzaoui K, Benmassaoud Y, Murtada K (2018) Magnetic nanocellulose from olive industry solid waste for the effective removal of methylene blue from wastewater. *Environ Sci Pollut Res* 25:22060–22074. <https://doi.org/10.1007/s11356-018-2107-y>
61. Tighadouini S, Radi S, Bacquet M, Degoutin S, Zaghrioui M, Jodeh S, Warad I (2016) Removal efficiency of Pb(II), Zn(II), Cd(II) and Cu(II) from aqueous solution and natural water by ketoenol-pyrazole receptor functionalized silica hybrid adsorbent. *Sep Sci Technol* 52:608–621. <https://doi.org/10.1080/01496395.2016.1262874>
62. Monti OLA (2012) Understanding interfacial electronic structure and charge transfer: an electrostatic perspective. *J Phys Chem Lett* 3:2342–2351. <https://doi.org/10.1021/jz300850x>
63. International Union of Pure and Applied Chemistry (IUPAC) (1997) Compendium of chemical terminology, 2nd edn. Blackwell Scientific Publications, Oxford (**The “Gold Book”**)
64. Benitex Y, Baranger AM (2011) Control of the stability of a protein–RNA complex by the position of fluorine in a base analogue. *J Am Chem Soc* 133:3687–3689. <https://doi.org/10.1021/ja102601h>
65. Saleh TA, Gupta VK, Al-Saadi AA (2013) Adsorption of lead ions from aqueous solution using porous carbon derived from rubber tires: experimental and computational study. *J Colloid Interface Sci* 396:264–269. <https://doi.org/10.1016/j.jcis.2013.01.037>

**Publisher's Note** Springer Nature remains neutral with regard to jurisdictional claims in published maps and institutional affiliations.

